Biophysical Chemistry 144 (2009) 130–135

Contents lists available at ScienceDirect

Biophysical Chemistry

journal homepage: http://www.elsevier.com/locate/biophyschem

Complex formation between calmodulin and a peptide from the intracellular loop of the gap junction protein connexin43: Molecular conformation and energetics of binding

Matti Myllykoski [a], Krzysztof Kuczera [b], Petri Kursula [a,*]

[a] Department of Biochemistry, PO Box 3000, FIN-90014, University of Oulu, Oulu, Finland
[b] Departments of Chemistry and Molecular Biosciences, University of Kansas. Lawrence, KS, USA

ARTICLE INFO

Article history:
Received 10 June 2009
Received in revised form 31 July 2009
Accepted 1 August 2009
Available online 7 August 2009

Keywords:
Calmodulin
Gap junction
Connexin43
Solution structure
Calorimetry
Regulation

ABSTRACT

Gap junctions are formed by a family of transmembrane proteins, connexins. Connexin43 is a widely studied member of the family, being ubiquitously expressed in a variety of tissues and a target of a large number of disease mutations. The intracellular loop of connexin43 has been shown to include a calmodulin binding domain, but detailed 3-dimensional data on the structure of the complex are not available. In this study, we used a synthetic peptide from this domain to reveal the conformation of the calmodulin-peptide complex by small angle X-ray scattering. Upon peptide binding, calmodulin lost its dumbbell shape, adopting a more globular conformation. We also studied the energetics of the interaction using calorimetry and computational methods. All our data indicate that calmodulin binds to the peptide from cx43 in the classical 'collapsed' conformation.

1. Introduction

Gap junctions are tight cell contacts, formed by transmembrane proteins of the connexin family, which allow for the diffusion of small molecules between adjacent cells. These intercellular channels are crucial for the transfer of, for example, metabolites, ions, and second messengers. Each gap junction is composed of two hemichannels, and each hemichannel in turn is formed of six connexin protein subunits. Connexins are a family of structurally related integral membrane proteins that share a similar architecture, having 4 transmembrane domains, two extracellular loops, and 3 cytoplasmic domains. The most ubiquitous connexin is connexin43 (cx43), which is expressed in a large number of different tissues and cell types [1].

A number of disease-linked mutations in cx43 have been reported. While the mutations are spread throughout the protein, a large fraction of characterized mutations in oculodentodigital dysplasia (ODDD) is found in the intracellular loop [2,3]. Also other connexins are disease-linked; for example, cx32 mutations cause X-linked Charcot–Marie–Tooth disease that severely affects the myelin sheath in the nervous system [4,5].

Since calmodulin (CaM) binding to gap junctions was discovered [6–9], a vast amount of studies have indicated that CaM is, indeed, involved in the calcium-dependent regulation of gap junction function. CaM has even been shown to be able to pass through a gap junction, possibly due to its elongated shape [10,11]. Cx43 has been shown to interact with CaM, and a specific binding site was recently [12] localised to the cytoplasmic loop, between residues 136–158. Similar sites have been characterized or suggested to be present in other connexins [13–17], indicating a putative general mechanism of gap junction regulation by CaM. Currently, no high-resolution data on the CaM-cx43 complex exist, and the sequence homology between cx43 and structurally characterized CaM target proteins is low.

CaM binds to its hundreds of target proteins usually in a calcium-dependent manner. The classical collapsed binding mode involves the wrapping of the peptide by the N- and C-terminal lobes of CaM, while the central linker helix is bent. During recent years, a growing number of divergent CaM-peptide recognition modes have been detected. The relationships between CaM conformation upon target peptide binding and function have been poorly characterized; thus, it is important to determine the 3D conformation of a CaM complex for any newly identified CaM target. Here, we set out to study the molecular conformation of the CaM-cx43 complex, for which no detailed 3D structural information has been available. Small-angle X-ray scattering (SAXS) and isothermal titration calorimetry (ITC) both strongly suggest that CaM adopts the collapsed conformation when it is bound to the CaM-binding domain of cx43.

* Corresponding author. Tel.: +358 44 5658288; fax: +358 8 5531141.
E-mail address: petri.kursula@oulu.fi (P. Kursula).

0301-4622/$ – see front matter © 2009 Elsevier B.V. All rights reserved.
doi:10.1016/j.bpc.2009.08.001

2. Materials and methods

2.1. Protein expression and purification

The synthetic 15-residue peptide representing the predicted CaM-binding site of human cx43, KVKMRGGLLRTYIIS (residues 144–158), was purchased from SBS Genetech, China. Calmodulin was expressed in *E. coli* from the pETCM vector [18] and purified using calcium-dependent affinity chromatography on phenyl sepharose, as previously described [19].

2.2. Small-angle X-ray scattering

Synchrotron SAXS data for CaM and the CaM-cx43-CBD complex were collected on beamline I711 at MAX-Lab, Lund, Sweden [20]. Data processing was done using the in-house Bli711 software, and

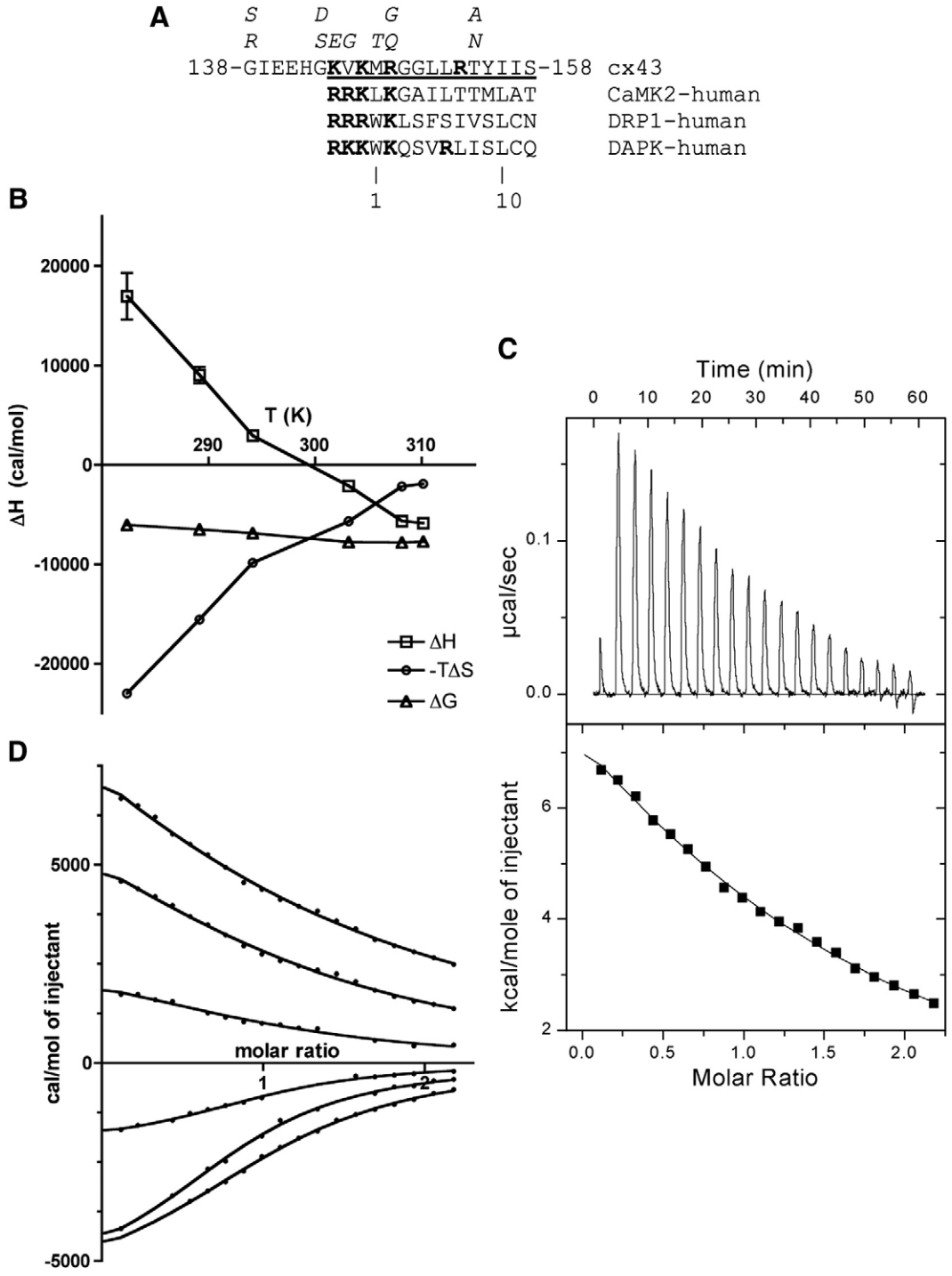

Fig. 1. The used peptide and its binding to CaM. A. Alignment of the cx43-CBD with CBDs from selected other proteins exhibiting a collapsed mode of binding. Known cx43 mutations within or near the CBD are also indicated in italics above the sequence. The peptide used in this study is underlined, and basic residues are highlighted in bold. B. The observed enthalpy as a function of temperature in ITC. The slope of the curve for ΔH allows the estimation of the heat capacity. C. An example of ITC titration and curve fitting of the CaM-cx43-CBD complex. The experiment was carried out at +9.2 °C; at low temperatures, the reaction is endothermic. D. Fitted ITC curves for all used temperatures, indicating a stoichiometry of 1:1. The temperatures are, from top (endothermic) to bottom (exothermic), +9.2, +16, +21, +30, +35, and +37 °C.

programs from the ATSAS package [21] were used for data analysis and molecular modeling.

2.3. Isothermal titration calorimetry

The interaction between CaM and the cx43 peptide was studied by ITC, using the VP-ITC equipment (Microcal Inc.). The experiment was carried out similarly under several different temperatures; the concentrations of CaM (in the cell) and the peptide (in the syringe) were 10.8 μM and 110 μM, respectively. Prior to the experiment, the protein and peptide were extensively dialyzed against the assay buffer (10 mM HEPES pH 7.5, 100 mM NaCl, 10 mM $CaCl_2$). Data analysis was carried out in Microcal Origin.

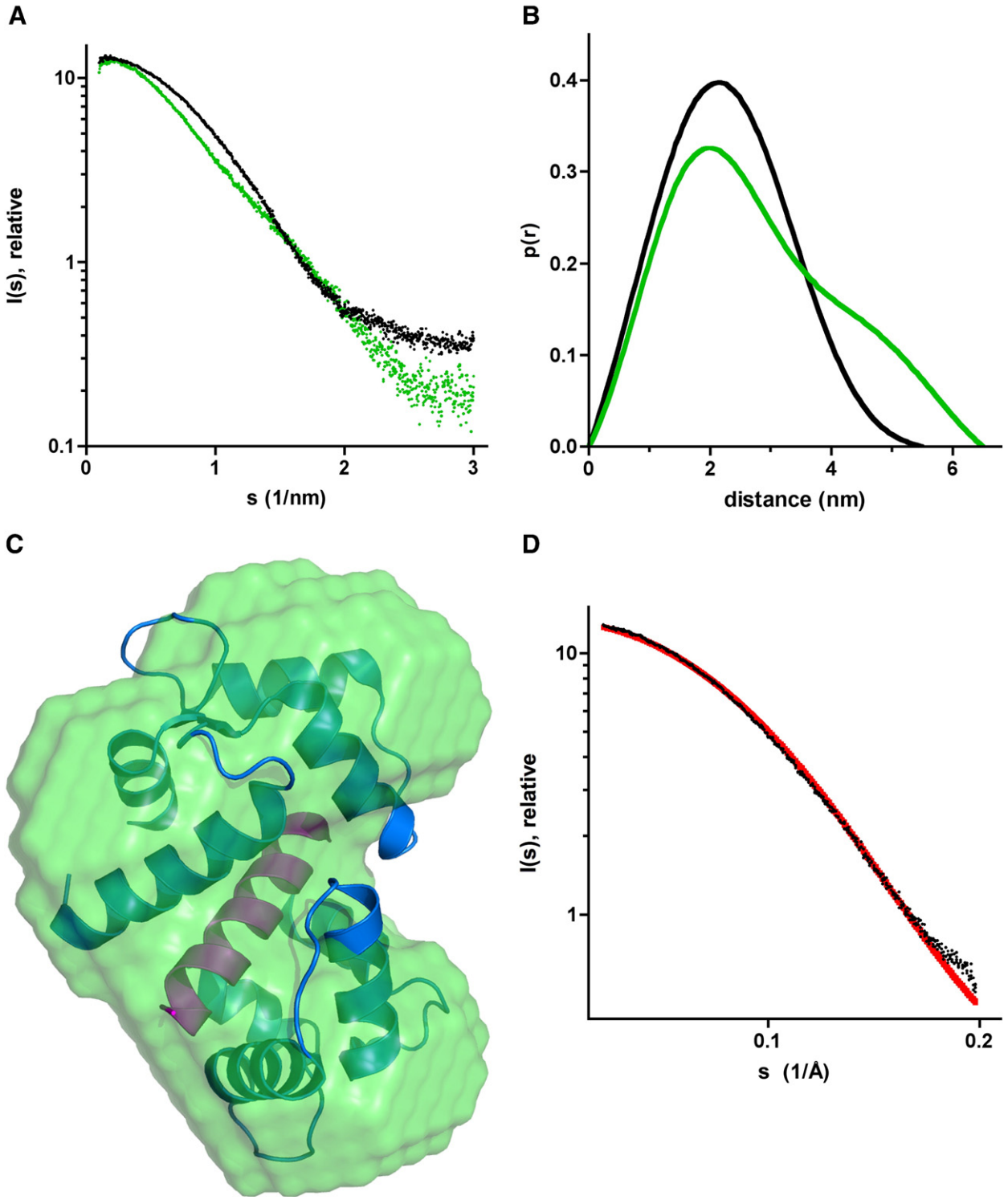

Fig. 2. SAXS of CaM and the CaM-cx43-CBD complex. A. Scattering curves. CaM is shown in green and the complex in black. B. Distance distributions from GNOM. Coloring as in A. C. *Ab initio* model for the complex obtained from DAMMIN (green), with the superimposed structure of the CaM-CaMKII-CBD complex (PDB entry 1CDM; CaM in blue and the peptide in red). D. Fitting of the theoretical scattering curve from 1CDM (red) to the measured curve (black) for the complex. (For interpretation of the references to color in this figure legend, the reader is referred to the web version of this article.)

Table 1
Results from SAXS and comparisons to theoretical values.

Sample	Rg (nm)	Dmax (nm)
SAXS:		
CaM	2.16	6.5
CaM + cx43	1.76	5.5
Crystal structures:		
1CDM	1.61	5.2
1UP5	2.29	7.0
1WRZ	1.70	5.4

1UP5, apo-CaM [32]; 1CDM, CaM complexed with a peptide from CaMKII [31]; and 1WRZ, CaM complexed with a peptide from DRP-1 kinase [33].

2.4. Molecular modeling

An initial model of the CaM-cx43-CBD complex was built using the sequence homology to DRP-1, and the corresponding crystal structure of CaM complexed to a mutant DRP-1 peptide (PDB entry 1ZUZ). The programs Coot [22] and Swiss-PdbViewer [23] were used for model construction and initial energy minimization, respectively. Thereafter, the complex was subjected to molecular dynamics (MD) simulations (see below).

2.5. Computational methods

The simulation followed the protocol earlier described [24]. Harmonic constraints were applied to the protein, using force constants of 10 kcal/(mol Å^2) for atoms within 6 Å, 15 kcal/(mol Å^2) for atoms within 6–11 Å and 30 kcal/(mol Å^2) for atoms further than 11 Å from the peptide. The CaM:cx43 peptide complex was energy minimized using 1000 steps of the ABNR method and next underwent 50 ps MD equilibration at 300 K. Finally, a 100-ps MD trajectory was generated at 300 K, with coordinates saved every 0.1 ps. The calculations did not include solvent; solvation was taken into account by using a distance-dependent dielectric constant = 1/4r.

The 1000 saved structures were used to calculate quantities of the type

$$\Delta X = \mathrm{X(CaM{:}cx43)} - \mathrm{X}(CaM) - \mathrm{X(cx43)}$$

where X(CaM:cx43) refers to the value of X in the complex, and X(CaM) and X(cx43) to the corresponding values for CaM alone and cx43 alone, respectively. All three quantities are obtained from the same structure, with only the selected atoms considered (single trajectory approximation). The trajectory averages were used to estimate binding free energies using two approximate formulas (values in kcal/mol):

$$\Delta G = 0.0335 < \Delta G_{\mathrm{PB}} > + 0.0016 < \Delta SASA > - 5.04 \quad \text{(a)}$$

$$\Delta G = -0.0028 < \Delta E_{\mathrm{elec}} > + 0.0399 < \Delta E_{\mathrm{vdW}} > - 7.63 \quad \text{(b)}$$

Here, ΔE_{elec} and ΔE_{vdw} are the CHARMM electrostatic and van der Waals energies, respectively, ΔSASA is the change in solvent accessible surface area, and ΔG_{PB} is the change in electrostatic free energy calculated with the Poisson–Boltzmann continuum electrostatic method. The optimized parameters in the above equations were obtained by fitting to experimental binding free energies of six CaM:peptide complexes with an RMS deviation of ca. 1 kcal/mol (P. Kursula, K. Kuczera, in preparation). All simulations were performed using the program CHARMM [25,26] and the version 22 protein topology and parameters [27].

3. Results and discussion

3.1. Binding of CaM to the 15-residue peptide from the cx43 intracellular loop

Previously, a longer peptide of 23 residues was used to detect a CaM-binding domain within the intracellular loop of cx43 [12]. Similar peptides were also studied in context of cx44/cx46 [17]. We decided to further map the binding domain on cx43 and used a much

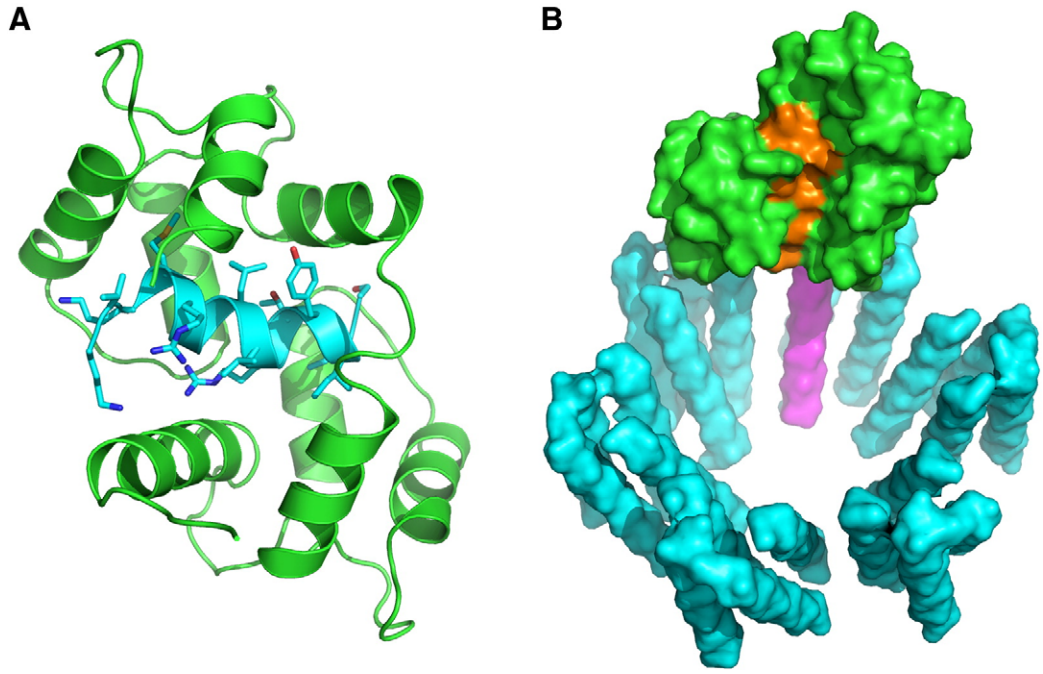

Fig. 3. Models of the CaM-cx43 interaction. A. Model of the CaM-cx43 complex. In this view, the cytoplasmic leaflet of the plasma membrane would be on the right hand side. B. The putative location of the CaM-binding site (orange) with respect to the entire gap junction (cyan). In theory, 6 CaM molecules (green) could be bound at the cytoplasmic face of cx43; the size of CaM is in the same range as the channel diameter. Helix 3 from one monomer is shown in magenta, with the orange CBD preceding it in sequence. (For interpretation of the references to color in this figure legend, the reader is referred to the web version of this article.)

shorter peptide of 15 residues, immediately before the 3rd transmembrane helix of cx43. Compared to the peptide previously used, this shorter peptide is missing, for example, two glycine and two glutamate residues, which can be assumed to be of little relevance to CaM binding. It should be noted that within the CBD and in the immediate vicinity of it, several characterized ODDD mutations are present, which could also affect CaM binding (Fig. 1A) [3].

Using isothermal titration calorimetry (Fig. 1B–D), it became obvious that the cx43-CBD bound to CaM in a 1:1 ratio (the fitted stoichiometry for the binding reaction was between 0.87 and 1.38 for all individual titrations), with an affinity in the low micromolar range (K_d between 2 and 12 μM for all experiments); the longer peptide was previously shown to have an affinity of approximately 1 μM [12]. We carried out the experiment at several different temperatures between +9 and +37 °C; the binding reaction was endothermic at low temperatures and exothermic at high temperatures. At low temperatures, the reaction is driven by a large favorable entropy.

From the analysis of enthalpy at different temperatures, we could estimate the heat capacity of the binding reaction. We, thus, can compare the cx43-CBD result to those obtained using other CaM-binding peptides in earlier studies. The estimated ΔCp for cx43, −3.6 kJ/mol (−850 cal/mol), is in the same range as average values, −3.2 kJ/mol, observed for peptides that are known to induce the so-called collapsed conformation of CaM around the peptide [28]. For peptides that mainly interact with only one lobe of CaM, the corresponding heat capacity is approximately half of that of a collapsed complex, −1.6 kJ/mol [28]. On the other hand, the complex between a peptide from MBP and CaM, which remains in an extended conformation, has a ΔCp in the range of −0.5 kJ/mol [29], indicative of an even smaller buried surface upon binding, and/or a different type of interaction. The ITC data strongly argue in favor of the option that CaM binds to the cx43-CBD in a closed conformation, enveloping the peptide tightly between its N- and C-terminal lobes.

3.2. Determination of the 3D solution structure of the CaM-cx43-CBD complex

In order to analyze the structural features of the CaM-cx43-CBD complex, we carried out a SAXS experiment for CaM in both the presence and absence of the cx43-CBD peptide. Already the raw scattering curves (Fig. 2A) indicated that the structure of the complex is significantly different from that of unliganded CaM. The calculated distance distributions (Fig. 2B) further indicated that the dumbbell shape of CaM is lost upon peptide binding, and the distribution indicates the presence of a more globular particle. This is also supported by the calculated radii of gyration and maximum particle diameter (Table 1). *Ab initio* modeling of the 3D structure was carried out for CaM and the complex using DAMMIN [30]. The results confirmed the presence of a dumbbell-shaped elongated unliganded CaM, and a collapsed conformation for the peptide complex (Fig. 2C).

Crystal structures of CaM and its respective peptide complexes could be superimposed on the *ab initio* structures with good fits. The result clearly indicates that CaM fully collapses around the cx43 peptide, in a 'classical' mode of binding. The best fit (Fig. 2D) was obtained for the complex between CaM and a peptide from CaM-dependent kinase II (CaMKII) [31], but in essence, all available collapsed CaM-peptide complexes fit to the SAXS data very well. For CaM without the peptide, a good fit to the corresponding crystal structure [32] was also obtained (data not shown), further confirming the conformational difference between the liganded and unliganded forms in solution.

3.3. Modeling of the cx43 structure

Using the structure of the complex of CaM with the DRP-1 S308D mutant peptide (PDB entry 1ZUZ), a model of the cx43-CBD bound to CaM was obtained (Fig. 3A). The structure shows the presence of residues Ile156 and Met147 in the hydrophobic pockets of the N- and C-terminal lobes of CaM, respectively. This binding mode is analogous to that seen for peptides from CaM-dependent protein kinases [31,33]. In addition, residues Lys144, Lys146, Arg148, and Arg153 are most likely involved in salt bridge interactions with acidic side chains from CaM. Unlike many other CaM-peptide complexes, it seems that there is no basic residue in cx43 that would interact with the acidic groups Asp80 and Glu84 at the bending region of the central helix. An analysis of the electrostatic and surface area contributions of key residues after the MD simulation is given in Table 2.

Considering the gap junction as a whole, the size of CaM is relatively large, taking also into account that a total of six CaM molecules could theoretically bind onto the cytoplasmic face of the hexameric cx43 hemichannel. Modeling of the Cα trace of the cx32 hemichannel suggested that it is transmembrane domain 3 which is mainly forming the inner face of the channel [34]; thus, the CaM-binding site studied here, being located immediately at the cytoplasmic side of this transmembrane domain in cx43, could, indeed be involved in gap junction regulation and conformational

Table 2
The calculated interaction free energy and buried surface area contributions from selected residues.

Electrostatic contributions (kcal/mol)		Buried surface area (Å^2)	
Calmodulin			
GLU 7	−1.5	GLU 7	45.1
GLU 11	−3.6	ALA 10	19.4
LYS 13	1.5	GLU 11	75.4
GLU 14	−3.4	GLU 14	36.7
GLN 41	1.1	ALA 15	25.6
ASP 80	2.9	LEU 18	10.4
GLU 84	1.2	PHE 19	43.2
GLU 114	−1.4	MET 36	32.3
GLU 120	−2.2	LEU 39	40.6
GLU 123	−2.0	GLN 41	44.5
GLU 127	−1.6	MET 71	15.2
LYS 148	2.1	MET 72	41.4
		LYS 75	31.9
		MET 76	81.0
		ASP 80	22.0
		GLU 84	16.9
		GLU 87	23.1
		ALA 88	42.5
		PHE 92	45.1
		LEU 105	14.2
		MET 109	23.2
		LEU 112	29.2
		GLU 114	17.5
		GLU 120	22.8
		MET 124	58.9
		GLU 127	12.3
		PHE 141	17.4
		MET 144	31.0
		MET 145	94.0
		LYS 148	59.7
Peptide			
LYS 144	−3.2	LYS 144	115.1
LYS 146	2.3	VAL 145	70.2
ARG 148	−7.7	LYS 146	140.7
ARG 153	1.1	MET 147	156.2
THR 154	1.1	ARG 148	74.6
TYR 155	2.8	GLY 149	14.6
SER 158	11.7	GLY 150	30.7
		LEU 151	62.6
		LEU 152	61.3
		ARG 153	165.9
		THR 154	85.6
		TYR 155	140.6
		ILE 156	135.9
		ILE 157	154.5
		SER 158	74.4

changes of cx43 related to it. A model of a CaM-bound gap junction built based on the above considerations is shown in Fig. 3B.

3.4. Concluding remarks

We have obtained 3-dimensional structural information on the complex between the cytoplasmic loop of cx43 and CaM, by means of synchrotron SAXS. Combined with our calorimetric and simulation data, our results unequivocally indicate that CaM collapses around its target sequence in cx43. Considering the gap junction as a whole, the CaM-binding site is in a position that may allow for the regulation of gap junction function by calcium signals *via* CaM. In the absence of high-resolution structural data for the complex, our data give a low-resolution glimpse into the complex and the likely location of bound CaM with respect to the whole gap junction, and provide a framework for further determining structure–function relationships between CaM and cx43.

Acknowledgements

This study has been supported by grants from the Academy of Finland, the Sigrid Juselius Foundation, and the Department of Biochemistry, University of Oulu. Data collection at MAX-Lab was supported by the European Community — Research Infrastructure Action under the FP6 "Structuring the European Research Area" Programme (through the Integrated Infrastructure Initiative "Integrating Activity on Synchrotron and Free Electron Laser Science"), contract RII3-CT-2004-506008 (IA-SFS). We thank Noora Löytynoja for helping in protein purification, and the staff of beamline I711 at MAX-Lab for excellent support during SAXS data collection.

References

[1] D.W. Laird, Life cycle of connexins in health and disease, Biochem. J. 394 (2006) 527–543.
[2] D.W. Laird, Closing the gap on autosomal dominant connexin-26 and connexin-43 mutants linked to human disease, J. Biol. Chem. 283 (2008) 2997–3001.
[3] W.A. Paznekas, B. Karczeski, S. Vermeer, R.B. Lowry, M. Delatycki, F. Laurence, P.A. Koivisto, L. Van Maldergem, S.A. Boyadjiev, J.N. Bodurtha, E.W. Jabs, GJA1 mutations, variants, and connexin 43 dysfunction as it relates to the oculodentodigital dysplasia phenotype, Human Mutat. 30 (2009) 724–733.
[4] J. Bergoffen, S.S. Scherer, S. Wang, M.O. Scott, L.J. Bone, D.L. Paul, K. Chen, M.W. Lensch, P.F. Chance, K.H. Fischbeck, Connexin mutations in X-linked Charcot–Marie–Tooth disease, Science 262 (1993) 2039–2042.
[5] C.K. Abrams, S. Oh, Y. Ri, T.A. Bargiello, Mutations in connexin 32: the molecular and biophysical bases for the X-linked form of Charcot–Marie–Tooth disease, Brains Res. Rev. 32 (2000) 203–214.
[6] C. Peracchia, S.J. Girsch, Functional modulation of cell coupling: evidence for a calmodulin-driven channel gate, Am. J. Physiol. 248 (1985) H765–H782.
[7] L.J. Van Eldik, E.L. Hertzberg, R.C. Berdan, N.B. Gilula, Interaction of calmodulin and other calcium-modulated proteins with mammalian and arthropod junctional membrane proteins, Biochem. Biophys. Res. Commun. 126 (1985) 825–832.
[8] C. Peracchia, G. Bernardini, L.L. Peracchia, Is calmodulin involved in the regulation of gap junction permeability? Pflugers Arch. 399 (1983) 152–154.
[9] M.J. Welsh, J.C. Aster, M. Ireland, J. Alcala, H. Maisel, Calmodulin binds to chick lens gap junction protein in a calcium-independent manner, Science 216 (1982) 642–644.
[10] R.A. Brooks, R.I. Woodruff, Calmodulin transmitted through gap junctions stimulates endocytic incorporation of yolk precursors in insect oocytes, Dev. Biol. 271 (2004) 339–349.
[11] J.E. Curran, R.I. Woodruff, Passage of 17 kDa calmodulin through gap junctions of three vertebrate species, Tissue Cell 39 (2007) 303–309.
[12] Y. Zhou, W. Yang, M.M. Lurtz, Y. Ye, Y. Huang, H.W. Lee, Y. Chen, C.F. Louis, J.J. Yang, Identification of the calmodulin binding domain of connexin 43, J. Biol. Chem. 282 (2007) 35005–35017.
[13] R. Dodd, C. Peracchia, D. Stolady, K. Torok, Calmodulin association with connexin32-derived peptides suggests trans-domain interaction in chemical gating of gap junction channels, J. Biol. Chem. 283 (2008) 26911–26920.
[14] C. Peracchia, A. Sotkis, X.G. Wang, L.L. Peracchia, A. Persechini, Calmodulin directly gates gap junction channels, J. Biol. Chem. 275 (2000) 26220–26224.
[15] C. Peracchia, X.G. Wang, L.L. Peracchia, Slow gating of gap junction channels and calmodulin, J. Membr. Biol. 178 (2000) 55–70.
[16] A. Sotkis, X.G. Wang, T. Yasumura, L.L. Peracchia, A. Persechini, J.E. Rash, C. Peracchia, Calmodulin colocalizes with connexins and plays a direct role in gap junction channel gating, Cell Commun. Adhes. 8 (2001) 277–281.
[17] Y. Zhou, W. Yang, M.M. Lurtz, Y. Chen, J. Jiang, Y. Huang, Calmodulin mediates the Ca2+-dependent regulation of Cx44 gap junctions, Biophys. J. 96 (2009) 2832–2848.
[18] N. Hayashi, M. Matsubara, A. Takasaki, K. Titani, H. Taniguchi, An expression system of rat calmodulin using T7 phage promoter in *Escherichia coli*, Protein Expr. Purif. 12 (1998) 25–28.
[19] P. Kursula, V. Majava, A structural insight into lead neurotoxicity and calmodulin activation by heavy metals, Acta Crystallogr., F Struct. Biol. Cryst. Commun. 63 (2007) 653–656.
[20] Y. Cerenius, K. Stahl, L.A. Svensson, T. Ursby, A. Oskarsson, J. Albertsson, A. Liljas, The crystallography beamline I711 at MAX II, J. Synchrotron Radiat. 7 (2000) 203–208.
[21] P.V. Konarev, M.V. Petoukhov, V.V. Volkov, D.I. Svergun, ATSAS 2.1, a program package for small-angle scattering data analysis, J. Appl. Crystallogr. 39 (2006) 277–286.
[22] P. Emsley, K. Cowtan, Coot: model-building tools for molecular graphics, Acta Crystallogr., D Biol. Crystallogr. 60 (2004) 2126–2132.
[23] N. Guex, M.C. Peitsch, SWISS-MODEL and the Swiss-PdbViewer: an environment for comparative protein modeling, Electrophoresis 18 (1997) 2714–2723.
[24] V. Zoete, O. Michielin, M. Karplus, Protein-ligand binding free energy estimation using molecular mechanics and continuum electrostatics. Application to HIV-1 protease inhibitors, J. Comput. Aided Mol. Des. 17 (2003) 861–880.
[25] B.R. Brooks, C.L. Brooks, A.D. Mackerell Jr., L. Nilsson, R.J. Petrella, B. Roux, Y. Won, G. Archontis, C. Bartels, S. Boresch, A. Caflisch, L. Caves, Q. Cui, A.R. Dinner, M. Feig, S. Fischer, J. Gao, M. Hodoscek, W. Im, K. Kuczera, T. Lazaridis, J. Ma, V. Ovchinnikov, E. Paci, R.W. Pastor, C.B. Post, J.Z. Pu, M. Schaefer, B. Tidor, R.M. Venable, H.L. Woodcock, X. Wu, W. Yang, D.M. York, M. Karplus, CHARMM: the biomolecular simulation program, J. Comput. Chem. 30 (2009) 1545–1614.
[26] B.R. Brooks, R.E. Bruccoleri, B.D. Olafson, D.J. States, S. Swaminathan, M. Karplus, CHARMM: a program for macromolecular energy, minimization, and dynamics calculations, J. Comput. Chem. 4 (1983) 187–217.
[27] A.D. MacKerell Jr., D. Bashford, M. Bellott, R.L. Dunbrack Jr, J.D. Evanseck, M.J. Field, S. Fischer, J. Gao, H. Guo, S. Ha, D. Joseph-McCarthy, L. Kuchnir, K. Kuczera, F.T.K. Lau, C. Mattos, S. Michnik, T. Ngo, D.T. Nguyen, B. Prodhom, W.E.R. Reiher, B. Roux, M. Schlenkrich, J.C. Smith, R. Stote, J. Straub, M. Watanabe, J. Wiorkiewicz-Kuczera, D. Yin, M. Karplus, All-atom empirical potential for molecular modeling and dynamics studies of proteins†, J. Phys. Chem., B 102 (1998) 3586–3616.
[28] R.D. Brokx, M.M. Lopez, H.J. Vogel, G.I. Makhatadze, Energetics of target peptide binding by calmodulin reveals different modes of binding, J. Biol. Chem. 276 (2001) 14083–14091.
[29] V. Majava, M.V. Petoukhov, N. Hayashi, P. Pirila, D.I. Svergun, P. Kursula, Interaction between the C-terminal region of human myelin basic protein and calmodulin: analysis of complex formation and solution structure, BMC Struct. Biol. 8 (2008) 10.
[30] D.I. Svergun, Restoring low resolution structure of biological macromolecules from solution scattering using simulated annealing, Biophys. J. 76 (1999) 2879–2886.
[31] W.E. Meador, A.R. Means, F.A. Quiocho, Modulation of calmodulin plasticity in molecular recognition on the basis of X-ray structures, Science 262 (1993) 1718–1721.
[32] B. Rupp, D.R. Marshak, S. Parkin, Crystallization and preliminary X-ray analysis of two new crystal forms of calmodulin, Acta Crystallogr., D Biol. Crystallogr. 52 (1996) 411–413.
[33] I. Bertini, P. Kursula, C. Luchinat, G. Parigi, J. Vahokoski, M. Wilmanns, J. Yuan, Accurate solution structures of proteins from X-ray data and a minimal set of NMR data: calmodulin-peptide complexes as examples, J. Am. Chem. Soc. 131 (2009) 5134–5144.
[34] S.J. Fleishman, V.M. Unger, M. Yeager, N. Ben-Tal, A Calpha model for the transmembrane alpha helices of gap junction intercellular channels, Mol. Cell 15 (2004) 879–888.